Bondline thickness: Fracture mechanics perspective

18

Sofia Teixeira de Freitas[a] *and Michal K. Budzik*[b]
[a]Aerospace Structures and Materials Department, Faculty of Aerospace Engineering, Delft University of Technology, Delft, Netherlands, [b]Department of Mechanical and Production Engineering, Aarhus University, Aarhus, Denmark

18.1 Introduction

Judging if the bondline is thick or thin is far from an easy task. For structural bonding, the common assumption is to consider the bondline as thin if its thickness is very small compared to the other dimensions of the joint. In doing so, we assume that the bondline thickness is much higher than, for example, the roughness of the joined surfaces, and thus, well above the atomic length scale. However, there is no absolute definition of a thick or thin bondline. For example, a 1-cm thick bondline will certainly be recognized as very thick by the aerospace industry where a few millimeters thick composite plates are bonded, but can be seen as a rather thin in civil engineering applications while bonding/joining concrete slabs or beams. Historically, motivated and driven by aerospace industry development of lightweight materials and structures, thin bondlines were of the highest importance and, thus, studied the most extensively. Thin bondlines have been assumed in building analytical models, as well as data reduction schemes and standards [1]. However, with the expansion of adhesive bonding to marine, wind energy, civil engineering, and other industries, thicker bondlines are encountered very often [2]. The number of works discussing the effects of adhesive layer thickness on the strength and toughness of the joint is considerable [3–12]. In these works, the thickness of the bondline ranges from nanometers to centimeters.

The early tests indicated the dependence of adhesive joint strength on adhesive thickness, for example [13], leading to conclusions often diverging from expectations. For instance, according to the continuum theory, an increase in adhesive thickness and, thus, its volume, should not affect the strength of the joint (strength, as we know, is derived from the cross section area of the joint and, thus, not related to the thickness) while the joint toughness should be improved (here, the thickness leads to a larger volume over which the energy flows). Contrary to this, the strength was shown to decrease with increasing the adhesive thickness. In a more recent study, such a decrease is observed once the so-called optimum bondline thickness is exceeded [10]. In addition, once the adhesive thickness increases above a certain value, the adhesive can be regarded as experiencing a three-dimensional stress state and critical stress gradients due to geometrical (edges and corner) and material (an adhesive is usually of different materials than the joined adherends) discontinuities [14–17].

Advances in Structural Adhesive Bonding. https://doi.org/10.1016/B978-0-323-91214-3.00027-2

The continuum mechanics stress analysis was no longer sufficient and the tools of fracture mechanics are now intertwined to fully comprehend and predict adhesive joint failure. Within the fracture mechanics framework and corner stress fields, pioneer works involving elastic-plastic analysis a joint revealed the existence of a critical thickness and of a plastic radius at the tip of the crack [18]. The following sections will be used to build a theoretical framework linking these two aspects with the adhesive thickness. The majority of the content will focus on fracture mechanics and will be built around the concept that the adhesive joint can store the mechanical energy within the adherends, within the bondline, or split between the two.

18.2 From thin to thick adhesive layers

Analysis of the adhesive joints can be divided into strength and toughness (or fracture) approaches, as discussed in detail in Chapter 14. Fig. 18.1A–C shows three typical test specimens often used to investigate strength and fracture in adhesive joints.

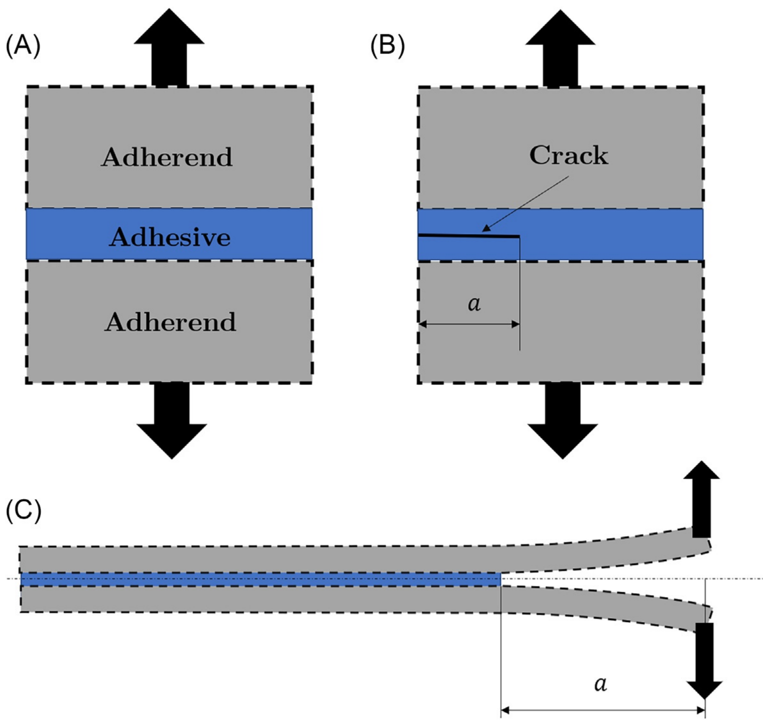

Fig. 18.1 Schematic representation of adhesively bonded specimens used to test the strength and toughness properties of joints. (A) The butt joint for testing strength; (B) the bonded single edge notch test (SENT) for testing fracture toughness; (C) the double cantilever beam (DCB) for testing fracture energy.

In the strength approach, such as using the butt joint in Fig. 18.1A, the focus is on evaluating the stress distribution and the stress level at which the bondline fails. The more general 3D stress analysis, for which limited closed-form solutions exist [19], can be reduced to the frequently used Volkersen and Goland and Reissner models developed for joints under shear loading [20, 21]. The details of such can be found in [22] as well as in Chapter 15 and will not be repeated here.

In the toughness approach, the interest lies in the measure of the energy levels at which the joints fail and the crack propagates. The fracture toughness, tested using single edge notch test specimens (SENT), as shown in Fig. 18.1B, is expressed in the units of stress per square root of length while the fracture energy, tested using the double cantilever beam (DCB) geometries, as shown in Fig. 18.1C is expressed in units of work per area.

These two toughness concepts, and the geometries proposed in Fig. 18.1A–C, will be used throughout this chapter to outline the importance of the energy flow through the adhesive joint. Looking to the extreme cases of both approaches, it is often the case that in the butt joint, the adherends can be assumed as perfectly rigid, thus not experiencing any deformations and not storing any energy, as shown in Fig. 18.1A and B. On the opposite extreme case, in the DCB-like specimens, as shown in Fig. 18.1C, the adhesive deformation is assumed negligible compared to the deformations experienced by the adherends.

Recall some of the small deformation continuum mechanics equations in which the stress tensor components σ_{ij} are defined as:

$$\sigma_{ij} = C_{ijkl}\epsilon_{kl} \tag{18.1}$$

where C_{ijkl} are the components of the stiffness matrix. For isotropic and elastic materials, the stiffness matrix components can be expressed through Young's modulus E and Poisson's ratio ν [23]. The associated strain tensor can be found from:

$$\epsilon_{ij} = \frac{1}{E^*}\left[\sigma_{ij} - \nu(\sigma_{kk}\delta_{ij} - \sigma_{ij})\right] \tag{18.2}$$

where $E^* = f(E, \nu)$ is material stiffness depending on, for example, the assumed stress state, and $\delta_{ij} = \begin{cases} 1 \ \forall \ i = j \\ 0 \ \forall \ i \neq j \end{cases}$ is the Kronecker's delta. Thus, under unidirectional applied stress, the strain field is not unidirectional and the so-called Poisson ratio effects can become visible once the adhesive thickness increases and the adhesive is characterized by a high Poisson's ratio. Such effects are important from both the strength and toughness perspectives, leading to rapid stress and strain gradients near the edge and the corner.

Consider butt joint testing using the specimen similar to the one shown in Fig. 18.1A in which the rigid adherends, $E \rightarrow \infty$, are joined with a relatively soft adhesive with modulus $E_a \ll E$, as illustrated in Fig. 18.2A. Experimentally, a force P or displacement Δ is applied to the adherends, leading to the stress inside the joint $\sigma_{zz} = \sigma_{zz}(x, y)$, that is, the load is perpendicular to the bondline, as shown in Fig. 18.2A $\rightarrow$ B′. Thus:

$$\sigma_{zz} = -\nu\left(\sigma_{xx} + \sigma_{yy}\right). \tag{18.3}$$

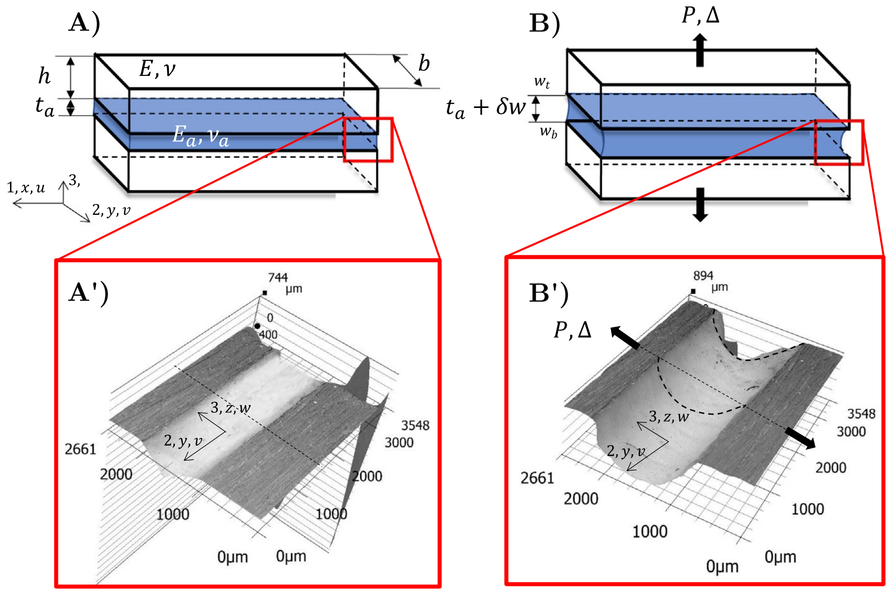

Fig. 18.2 (A) Schematic representation of the butt joint before the load is applied and (A′) the corresponding picture of the edge and corner vicinity obtained using three-dimensional scanning microscopy. (B) and (B′) The same specimen but after the remote tensile load is applied. (B′) emphasizes the role of Poisson's ratio. In the experiment, the joint consisted of aluminum blocks bonded with methyl methacrylate (MMA) adhesive with $\nu_a = 0.45$.

This configuration, being only one of the versions of the butt joint, is usually regarded as a simple and convenient test to evaluate bondline strength. During the loading, the strain in the thickness direction is given by $\epsilon_{zz} = (w_t - w_b)/t_a$, where w_t and w_b are the displacements of the top and bottom adherends and t_a is the initial thickness of the adhesive; see Fig. 18.2. At the center of the adhesive layer, the σ_{ii} stress components are building up due to a nonzero Poisson's ratio, that is, Eq. (18.3). However, along, for example, the adhesive/adherend interface, assuming that the adherend material can be considered as nondeformable, the Poisson's ratio contraction is unconstrained, leading to visible bondline deformation, as shown in Fig. 18.2, A′ → B′.

Additional shear components, σ_{ij} with $i \neq j$, are thus present. Consequently, strains, and stresses, must be functions of position within the adhesive layer, including through the adhesive thickness direction. The distance and the associated load transfer over which the strains and stresses vary give through the thickness direction rise to the vivid studies of confinement and constraint effects [24, 25].

18.2.1 Energy approach and fracture mechanics

Fracture mechanics dates back to the work of Griffith, who used the energy approach to describe the failure of brittle, elastic solids [26]. Many of the initial works focused on applying Griffith balance to adhesive joint geometries [27–29]. Consider the total elastic energy stored in the adhesive joint as U being the sum of energies stored in the adhesive U_a and the adherends U_b, i.e., $U = U_a + U_b$. For the butt joint geometry presented in Fig. 18.2 and a material system such that $E_a \ll E$, that is, the extreme case where the adherends can be considered as rigid, the total energy is given to the one stored in the elastic adhesive layer, U_a (as $U_b \approx 0$), and can be defined as:

$$U \equiv U_a = \frac{1}{2}\int_V \sigma_{ij}\epsilon_{ij}dv = \frac{1}{2}bt_a\int_l \sigma_{ij}\epsilon_{ij}dx \tag{18.4}$$

with v being adhesive layer volume, and l and b being the extension of the bonded region along the x and y directions, respectively. Acknowledging the limitations of the above approach, we observe that the stored energy is proportional to the adhesive thickness. Ignoring effects due to the kinetic energy, or the plastic zone dissipation, we define the elastic strain energy release rate (SERR or ERR for short):

$$\mathcal{G} = -\frac{dU}{dA} \tag{18.5}$$

where A is the surface area of the crack. For geometries with constant width b (such as those usually used for testing) where the crack propagated the distance a, $A = ba$. Notice that because we consider an elastic case and assuming laboratory loading conditions through controlled displacement, the stored energy balances out the work done by the external forces.

Consider now a fracture mechanics derivative of the butt joint—SENT specimen geometry depicted in Fig. 18.3A. Let us examine the material case studied previously, i.e., the adherend deformation is very small compared to the deformation of the bondline, $U \approx U_a$ under the remote stress field $\sigma_{ij}\epsilon_{ij} = \sigma\epsilon$, see Fig. 18.3B. Combining Eqs. (18.4) and (18.5) yields:

$$\mathcal{G} = \frac{1}{2}t_a\frac{d}{da}\left(\int_a^l \sigma\epsilon dx\right) \propto t_a \tag{18.6}$$

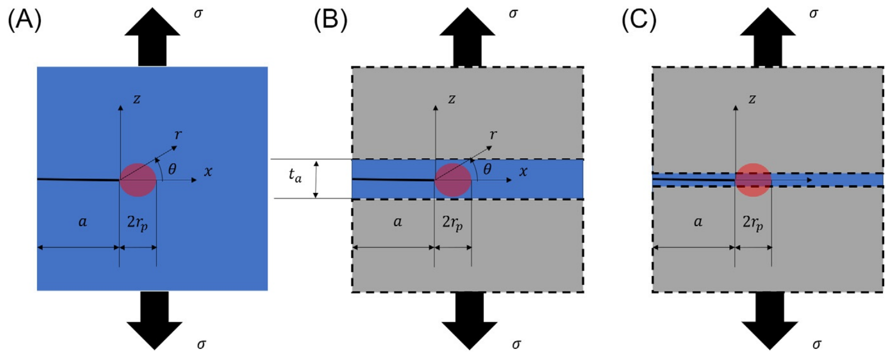

Fig. 18.3 A schematic representation of (A) a specimen with a side crack of length a, under remote loading σ—the SENT fracture specimen, (B) SENT with thick and (C) thin adhesive layer.

with l corresponding to the length of the adhesive layer. The result is equivalent to the one derived by Gent [30] for "soft" adhesives. The $\mathcal{G}$ depends on the adhesive thickness and increases until fracture. In a generic manner, $\mathcal{G} = \mathcal{G}_c$ once the crack begins to propagate defining the Griffith's fracture criterion. $\mathcal{G}_c$ is called the fracture energy and for isotropic, homogeneous materials it is deemed as material constant under the assumption of equilibrium and a self-similar fracture process. While we can be encouraged by the simplicity of the solution, unfortunately adhesive joints are not homogeneous materials but structures, and thus, the presented theory needs further refinement.

18.2.2 Stress near the crack tip and emergence of material length scale

With the details behind fracture mechanics provided in Chapters 14 and 16, let us return to the SENT specimen and consider the testing of a homogeneous material, such as a bulk adhesive, under remote Mode I loading conditions; see Fig. 18.3A. Assuming the plane stress conditions at the crack tip for the sake of simplicity, the Mode I stress field is described as [31–33]:

$$\sigma_{zz} = \frac{K_I}{\sqrt{2\pi r}} \cos\frac{\theta}{2}\left(1 + \sin\frac{\theta}{2}\sin\frac{3\theta}{2}\right) + \cdots \tag{18.7}$$

where r and θ are the distance from the crack tip and the angle measured from the expected crack growth plane, respectively. The K_I is called the Mode I stress intensity factor that at the crack onset, yields $K_I \equiv K_{Ic}$. K_{Ic} is defined as the fracture toughness and it is regarded as a material constant. The dropped higher order terms, indicated in Eq. (18.7) by the dots, become negligible as $r \to 0$ and practically as $r \leq 0.1a$. For $r \to 0$, the elastic solution tends to a nonphysical infinite stress denoting mathematical singularity. For large r, the solution ceases and the stress level converges to the Saint-Venant simplification.

The toughness, or resistance to crack growth, of a material is governed by the energy dissipated during the fracture process. For the perfect elastic-brittle materials, such as Griffith's materials, like glass, this energy can be deduced from the rupturing energy of primary chemical bonds. This is not the case for structural adhesives where a large damage zone in front of the crack front is likely to develop; toughening strategies for adhesives are discussed in detail in Chapter 8. In this zone, a significant amount of energy will be dissipated, usually of orders of magnitude higher than the energy predicted by atomic bonding calculations.

Returning to the discussion of the SENT specimen fracture, we assume a physical limit to the stress due to a plastic limit, that is, $\sigma(r=0) = \sigma_y$ such that $\sigma = \sigma_y \; \forall \; r \leq r_p$ where r_p defines the region in which a material undergoes plastic deformation. Substituting σ_y and r_p into Eq. (18.7), after rearrangement:

$$2r_p = n\frac{K_{Ic}^2}{\sigma_y^2}. \tag{18.8}$$

Eq. (18.8) defines an intrinsic material property initially derived by Irwin [34] and an important material length scale. In addition, $K_{Ic}^2 = E^* \mathcal{G}_c$, thus, $\mathcal{G}_c \propto r_p$—the fracture energy is a measure of the plastic radius, or the plastic radius is a measure of resistance to fracture. n, stated explicitly in Eq. (18.8), is a constant of order 1 that can be attributed to the current crack tip stress state. However, the existence of r_p holds important implications for adhesive joints.

Consider that the adhesive occupies a finite domain of thickness t_a with material properties (E_a, ν_a) significantly different than the surrounding (E ν) and that $E_a \ll E$ and $\nu_a \geq \nu$, as in most practical cases Taking t_a and r_p interactions, the following cases can be recognized: if $t_a > r_p$, both length scales can coexist without affecting each other, and for example increasing t_a does not increase r_p; see Fig. 18.3B; once $t_a \leq 2r_p$, as shown in Fig. 18.3C the stress distribution in the crack tip region will be altered by t_a promoting the high level of stress triaxiality along the bonded plane [24, 25]. In the limit case of $t_a \approx 0$, the adhesive layer can be regarded as the crack growth plane, justifying an initial, aerospace-motivated approach to adhesive joint analysis. It is now well understood that the adhesive confinement affects the evaluated values of fracture parameters and this has been related with the altering of the development of the plastic zone [18, 35–37].

18.2.3 Edge and corner stress fields

The previously outlined analysis was not explicitly concerned by the fact that the stress and the strain vary in the vicinity of the interfaces between the two materials [14], that is, the edge and the corner effects. For SENT geometries, for example, such simplification is only justified if $t_a < a$ and $t_a > 2r_p$, but not otherwise. This disclosure is very important, as just after joint manufacturing $a \approx 0 < t_a$ is deemed. For DCB geometries, as depicted in Fig. 18.4, we can assume $t_a \ll a$ only if $t_a < r_p$. The bottom row of Fig. 18.4 shows the (tensorial) shear strain component ϵ_{xz} gathered for the three t_a cases (from the left): $t_a \ll 2r_p$; $t_a \approx 2r_p$, and; $t_a > 2r_p$ using digital image correlation (DIC) (see Chapter 32 for details about the DIC technique). Only color maps (the same shear strain range is used for all the cases) are given, limiting our discussion to the qualitative.

In this example, an elasto-plastic adhesive has been used to bond two aluminum adherends. Significant differences between the three cases are recorded. For $t_a \ll 2r_p$, as shown in Fig. 18.4A, the shear stresses are forming the so-called shear bands inside the adherends. A single stress field can be associated with the crack tip. The energy is then stored mainly in the adherends, and the bondline can be effectively seen as a crack growth plane. For the $t_a \approx 2r_p$, as shown in Fig. 18.4B, the intensity of the shear band inside the adherends decreases, the marking the fact that more of the deformation occurs within the adhesive layer. However, with similar resolution of the DIC results as in the previous case and contrary to a single crack tip field, the strain localizes near the corners. The energy is thus distributed between the adhesive and the adherends. Finally, for the $t_a > 2r_p$, as shown in Fig. 18.4C, the adherends do not experience significant deformation compared to the adhesive. The adhesive corners and, at

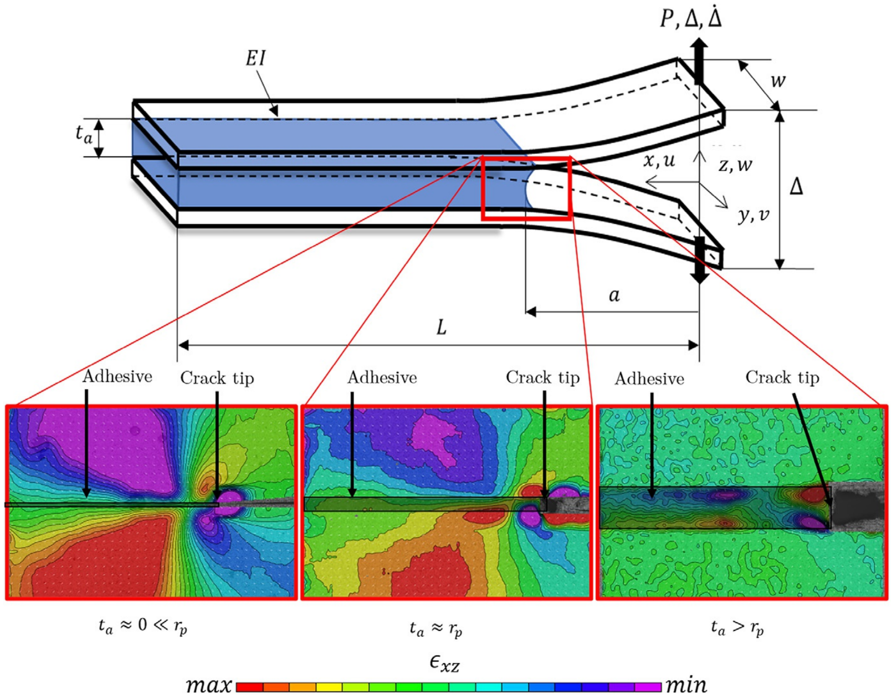

Fig. 18.4 Comparison of ϵ_{xz} shear strain field near the crack front for the joints with different adhesive thicknesses. *Top row*: Schematic representation of DCB specimen used for testing. *Bottom row*: The results obtained with the two-dimensional DIC, for the three adhesive thickness cases (from left): $t_a = 0.5$ mm $\ll 2r_p$; $t_a = 2.5$ mm $\approx 2r_p$, and; $t_a = 10$ mm $> 2r_p$.

some distance away, the adhesive/adherend interface are localizing the strains. As depicted in Fig. 18.4, and recognized in [36], two main mechanisms of plastic dissipation in adhesive joints exist: dissipation at the crack tip inside the r_p, and shear near corners and edges. Using the same adhesive material in the same geometrical configuration of the adherends under the same loading conditions, the failure localization and failure load can be regarded as controlled by the adhesive thickness. The corners and the edges are often crack onset locations and are likely to become growth paths, as will be further shown in this chapter by experimental results. The stress intensity factor and the crack tip stresses need to be quantitatively linked with the adherends, or specifically with the adhesive/adherend properties mismatch. Mathematically, the resulting stresses have a complex form, and, for Mode I loading, the real part reads as:

$$\sigma = \mathcal{R}\left(K r_{\varepsilon}^{-1/2+i\varepsilon}\right) \tag{18.9}$$

where $\varepsilon = \frac{1}{2\pi}\ln\left(\frac{1-\beta}{1+\beta}\right)$ is the bi-material exponent [16] dependent on the Dundurs parameter β [15]. For completeness, both Dundurs parameters are defined as [38]:

$$\alpha = \frac{(1-\nu_2)/\mu_2 - (1-\nu_1)/\mu_1}{(1-\nu_2)/\mu_2 + (1-\nu_1)/\mu_1}, \tag{18.10}$$

$$\beta = \frac{1}{2}\frac{\mu_1(1-2\nu_2) - \mu_2(1-2\nu_1)}{\mu_1(1-\nu_2)+\mu_2(1-\nu_1)}, \tag{18.11}$$

with $\mu_i = \frac{E_i^*}{2(1+\nu_i)}$, and $E_i^* = \begin{cases} E \text{ plane stress} \\ \frac{E}{1-\nu_i^2} \text{ plane strain} \end{cases}$ [17].

Contrary to the homogeneous case, a pair of bi-material constants α and β is introduced linking the respective ν_i and E_i^*. As the contrast between the joined materials increases, the stress gradient near their edge and corner increases. Once the mismatch vanishes, the homogeneous material solution, as shown in Eq. (18.7) is recovered. The results, such as in [16], indicate that the failure load decreases upon increasing the bondline thickness even above the $t_a \gg 2r_p$. To complete discussion, we acknowledge that the corner, or 3D singularity, is "stronger" than the edge, two-dimensional (2D), ones [39]. Fig. 18.5A and B schematize the emerging corner stress field.

The situation depicted arises if t_a is large enough so that the stress fields, distributed over r_ε, as shown in Eq. (18.9) from each corner, do not interact. As in the case of crack tip singularity and r_p, as $t_a \to 0$, the corner stresses are constrained between the adherend material. Under such circumstances, the crack will likely initiate in the middle of the adhesive layer. The situation becomes more complex once both r_p and r_ε coexist [40].

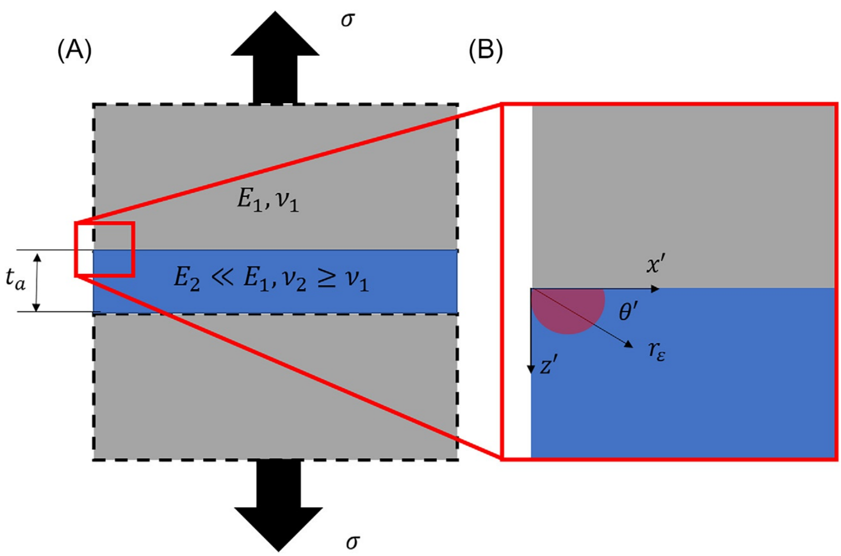

Fig. 18.5 Schematic representation of Mode I stress field near the bi-material corner. (A) The butt joint under remote tensile loading σ. (B) Close-up on the corner region where a local stress field emerges.

18.3 Adhesive thickness analysis using double cantilever beam (DCB) configuration

18.3.1 The adhesive/adherend energy flow

In the following sections, the effect of adhesive thickness on effective fracture properties obtained from DCB testing will be discussed. With the geometry defined in Fig. 18.4, following the simple beam theory [41], the compliance C is expressed as:

$$C \equiv \frac{\Delta}{P} = \frac{2a^3}{3EI}. \tag{18.12}$$

where the adherend is characterized via the beam bending rigidity $EI = E\frac{bh^3}{12}$. No explicit term for the adhesive layer is provided with the assumption that only the adherend is deforming and, thus, storing energy, implying $a \gg t_a$ and $t_a < r_p \approx 0$. The total elastic energy becomes $U = U_b = \frac{1}{2}P\Delta = \frac{1}{2}P^2C$ and marks the second extreme case for which the adhesive deformation is ignored. Substituting U_b into Eq. (18.5) we obtain:

$$\mathcal{G} = \frac{1}{2}\frac{P^2}{b}\frac{\partial C}{\partial a} \tag{18.13}$$

expressing the essence of the compliance method for calculating $\mathcal{G}$ and with Eq. (18.12) yielding:

$$\mathcal{G} = \frac{1}{2}\frac{P^2}{b}\frac{a^2}{EI}. \tag{18.14}$$

Substituting for rectangular cross section bonded adherends, $I = bh^3/12$:

$$\mathcal{G} = 12\frac{P^2a^2}{Eb^2h^3}. \tag{18.15}$$

The adhesive layer contribution is not included, but this should not imply it is not affecting the results; the adhesive layer plays a role in stress and energy flow.

Assuming equilibrium crack growth conditions, $\mathcal{G} = \mathcal{G}_c = const.$, the amount of energy released from both the adherend and the adhesive should be constant, thus:

$$-\frac{dU_b}{bda} + \frac{1}{2}t_a\frac{d}{da}\left(\int_a^l \sigma_a\epsilon_a dx\right) = \mathcal{G}. \tag{18.16}$$

For the beam problem investigated, the second term on the left side needs to be evaluated from the spatially varying stresses and strains within the adhesive layer, that is, $\sigma_a \wedge \epsilon_a = f(x)$. This is rarely performed. One of the well established frameworks mitigating such evaluation is called the effective crack length approach [42, 43]. In this approach, the integral term, related to the adhesive layer, becomes part of a lumped parameter a_e, and expressing the effective crack length that differs from the actual, observed, or apparent one, a. In specific, $a_e > a$ due to the finite stiffness of the adhesive layer not captured by Eq. (18.15). Taking an adhesive of stiffness E_a, increasing t_a leads to bigger a_e. Such a value is then used in Eq. (18.15) instead of a. Not following such a procedure leads often to significant misinterpretations. Eq. (18.16) is however aimed at expressing an important concept and paradigm. Considering stress and fracture analyses, it is important to recognize where the energy is stored, either in the adhesive, as in Eq. (18.4), or the adherend, as in Eq. (18.14), or a combination of the two, as in Eq. (18.16). We usually follow only one of the two extreme paths. Some analyses assume the adhesive layer to be sufficiently thin, such as simple beam theory for DCB (Eq. 18.14), while others assume just the opposite, for example, soft adhesives with rigid adherends for which all the energy is stored in the adhesive and this drives the fracture; Eq. (18.6). While these approaches can be very appropriate in very specific situations, the adhesive thickness is one the geometrical length scales that easily converts one into another. One of the models enabling treatment of both cases is based on the assumption that the bondline can be represented as a continuous series of springs, resulting in the beam on elastic foundation formulation.

18.3.2 Interpretation using elastic foundation models

The popularization of laminated composite materials required improved representation of interfaces, for example through the so-called elastic foundation models [44]. The foundation, or the interface/bondline as in our case, is represented by the distributed springs. Such an idea have been implemented successfully to many problems related to composites and adhesive bonding to predict stresses in the vicinity of the crack front [21, 45–48]. The well-recognized model is due to Kanninen [49]. Originally devised within the context of crack onset and arrest in laminated composite material, it proposes the governing beam problem to be formulated as:

$$\frac{d^4w}{dx^4} + 4\lambda^4 H(x)w = 0 \tag{18.17}$$

where $w(x)$ is the searched solution of the beam deflection, $H(x)$ is the Heaviside step function valued as:

$$H(x) = \begin{cases} 0 \ \forall \ x < a \\ 1 \ \forall \ x \geq a \end{cases} \tag{18.18}$$

and $\lambda = \lambda_{MK}$ is found from:

$$\lambda_{MK}^4 = \frac{k_{MK}}{4EI} \tag{18.19}$$

This is obtained from the characteristic root of the governing equation, Eq. (18.17), with the physical interpretation of the wave number. The inverse of λ is denoting the length of the region over which significant tensile stresses, are distributed.

Usually, this region is much longer than the validity of the local, asymptotic analysis, given by Eq. (18.7). If laminated material is considered, the thickness of the interface is assumed to be 0, and the constant k, i.e., the effective stiffness of the interface, can be associated with the (finite) transverse stiffness of the beam material. For instance, for the case of a beam made of isotropic material with a rectangular cross section of width b and thickness h, $k = \frac{2Eb}{h}$ under the assumption that the stresses can develop within the half of the beam thickness:

$$\lambda_{MK} = \frac{\sqrt{6}}{h}. \tag{18.20}$$

We should not disregard this solution. Even if $t_a \approx 0$, but adherends such as composite or wood (in general, materials with transverse properties similar to the one of the bondline material) are bonded, the Kanninen model can be used successfully. To the first approximation, the stress inside the bonded region can be evaluated from:

$$\sigma_{zz}(x) = E\epsilon_{zz} = \frac{k_{MK}}{b} w(x) = \frac{E}{2}\frac{w(x)}{h} \propto Ee^{-\lambda x}. \tag{18.21}$$

This analysis considerably affected the field of adhesion and bonding, and the approach has ever since been followed, expanded, and recently reviewed [48]. For adhesive bonding, in most cases the effective adhesive layer stiffness is significantly lower than that of the adherend, owing either to the increased thickness or much lower modulus of elasticity. Thus, representation of the adhesive layer as the elastic foundation while ignoring transverse adherend stiffness can be found in [17, 21, 46] to list only a few positions. We follow the analysis provided in [17] where the effective foundation stiffness is approximated by $k_{SK} = \frac{E_a'}{t_a}$ with $E_a{}'$. Accounting for the plane strain conditions in the adhesive layer, that is, $E_a' = E_a(1 - \mu_a^2)$, from Eq. (18.17) with $\lambda => \lambda_{SK}$:

$$\lambda_{SK}^4 = \frac{6}{t_a h^3}\frac{E_a'}{E}. \tag{18.22}$$

The adhesive thickness is explicitly introduced and controls the region of nonzero beam curvature (i.e., link to the effective crack length approach) and, equivalently, the stress distribution within the adhesive layer, namely λ_{SK}^{-1}. Carrying out the ERR derivation, Eq. (18.5) yields:

$$\mathcal{G} = \frac{1}{2}\frac{(Pa)^2}{bEI}\left(1 + \frac{1}{\lambda_{SK} a}\right)^2 \tag{18.23}$$

We notice that contrary to the monomial form of Eq. (18.15), a polynomial form of a more general Eq. (18.16) is restored. In specific, the second term on the right side is linked with the integral, i.e., the adhesive, term of Eq. (18.16), while the first term with the beam bending, dU_b/da. Indeed, setting $\lambda_{SK}a \gg 1$ in the denominator of Eq. (18.23), the second term approaches 0 and the entire bracket approaches unity. Eq. (18.14) can then be seen as an asymptotic solution for $U \to U_b$ and any nonzero adhesive thickness and stiffness will lead to misinterpretations if the limit, beam analysis, is used.

18.4 Effect of adhesive thickness on failure modes and fracture properties

18.4.1 Case study from thin to thick

The case study hereby presented focuses on the adhesive bondline thickness effect on Mode I fracture behavior of steel-to-steel bonded joints. A structural epoxy adhesive with bondline thicknesses from 0.4 to 10 mm is investigated using the DCB test. The case study becomes relevant for the application of structural adhesive bonding in maritime and civil engineering structures. The manufacturing tolerance in such structures can lead to "extra" thick bondlines in the order of centimeter scale. In this section the main findings of this case study are described. The detailed experimental procedure can be found in [50]. The adhesive used was a bi-component epoxy paste Araldite 2015 (Huntsman). First the influence of the adhesive thickness on the failure modes, fracture toughness values, and stress field ahead of the crack tip are shown. These results are then used to discuss and justify the trend of the fracture toughness. Finally, a few considerations are given regarding the strain rate dependency with the adhesive thickness.

18.4.1.1 Failure modes

Fig. 18.6 gives an overview of the crack path for representative specimens of 0.4, 1.1, 4.1, and 10.1 mm. Firstly, it can be observed that the crack path did not follow the mid-plane of the adhesive layer. This alternating crack path, recognized in the prior literature, such as [51, 52], is more pronounced with the increasing thickness, with the

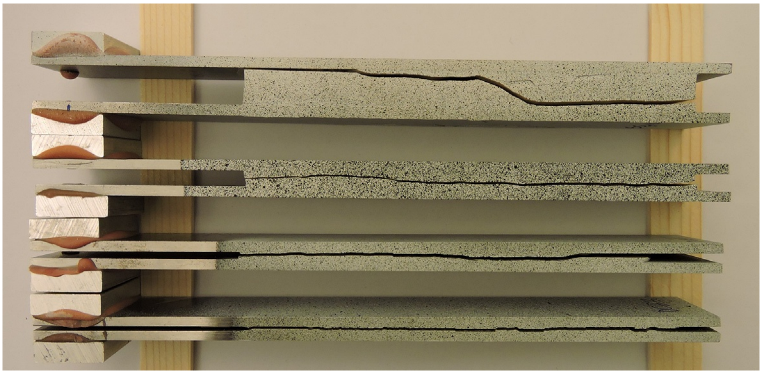

Fig. 18.6 Typical failure modes of each bondline thickness (from bottom to top: 0.4, 1.1, 4.1, 10.1 mm).

extreme case being the 10.1 mm thick adhesive layer where the crack path deflected from one interface to the other. Despite the alternating crack path, the failure was consistently cohesive owing to robust surface treatment procedure, i.e., no interface failure was observed. A more quantitative representation of the crack path profile for different positions along the specimen width (y) is shown in Fig. 18.7. For each adhesive thickness, one representative specimen is presented.

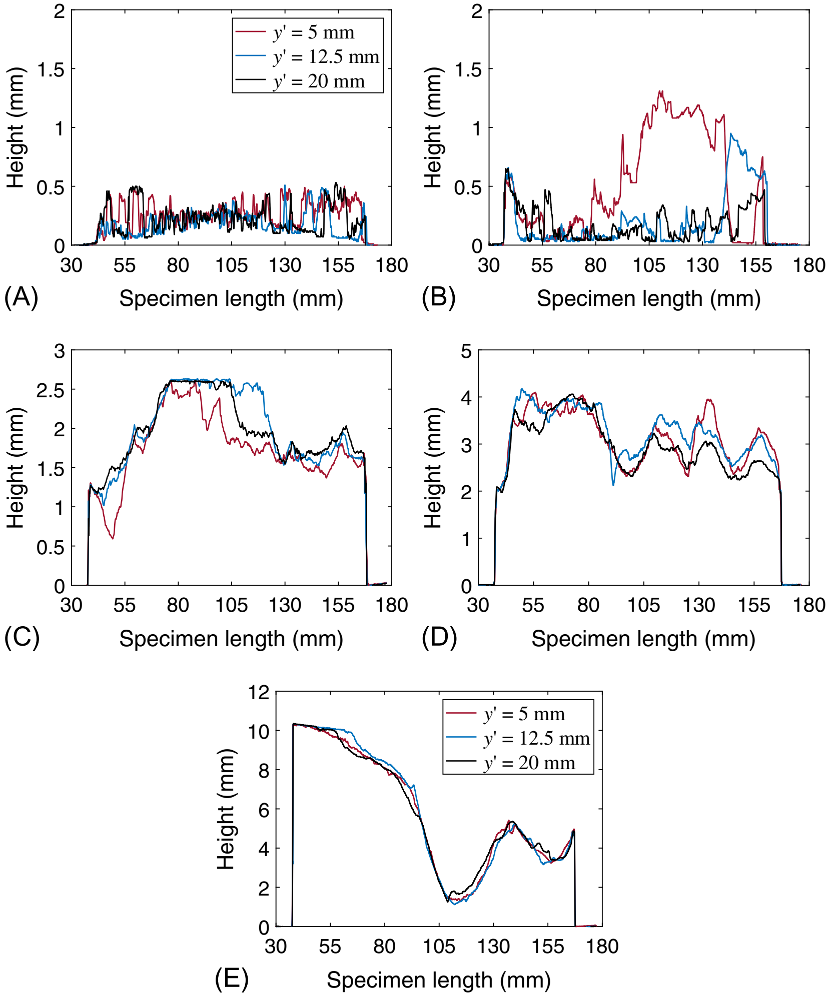

Fig. 18.7 Height profile (0 is position of the interface) of the remaining adhesive layer on the failure surface in respect to the reference adherend surfaces along the specimen's length direction of the representative specimens: (A) Bondline thickness ($t_a = 2t$) of 0.4 mm; (B) $t_a = 2t = 1.1$ mm; (C) $t_a = 2t = 2.6$ mm; (D) $t_a = 2t = 4.1$ mm; (E) $t_a = 2t = 10.1$ mm. The height profile is plotted at $y' = 5$, 12.5 and 20 mm, where y' is the coordinate in the specimen width direction [50]. Notice, that the adhesive thicknesses deviations along the specimen length justify the few cases where the height profile is higher than the average adhesive thickness.

18.4.1.2 Fracture energy

Fig. 18.8 gathers the fracture energy values as a function of the adhesive thickness. The fracture energy was determined using the elastic foundation models described earlier, as in Eq. (18.23), considering 3D plane strain.

18.4.1.3 Stress fields ahead of the crack tip

Besides the values for fracture energy in Fig. 18.8 the predicted deformation zone ahead of the crack tip of each bondline thickness is also plotted as $2r_p + \lambda_{j-\exp}^{-1}$ where $j = 0.4, 1.1, 2.6, 4.1, 10.1$ mm and $\lambda_{j-\exp}^{-1}$ corresponds to the value of the experimental λ^{-1} of thickness of j mm, that is, the length of the elastic process zone; see Eq. (18.22). The value $2r_p$ corresponds to the plastic process zone length; see Eq. (18.8). For the given case, this value is equal to 1.08 mm, assuming the plane strain conditions. The energy dissipation mainly occurs in the plastic deformation zone. However, the elastic process length also affects the recorded externally applied displacement. The experimental elastic fracture process length, $\lambda_{j-\exp}^{-1}$ was determined using experimental data, load, and crack length, and was defined as the distance over which the positive peel stress is distributed up to the yield strength of the bulk adhesive. Fig. 18.9 shows the peel stress ahead of the crack tip derived using Eq. (18.21).

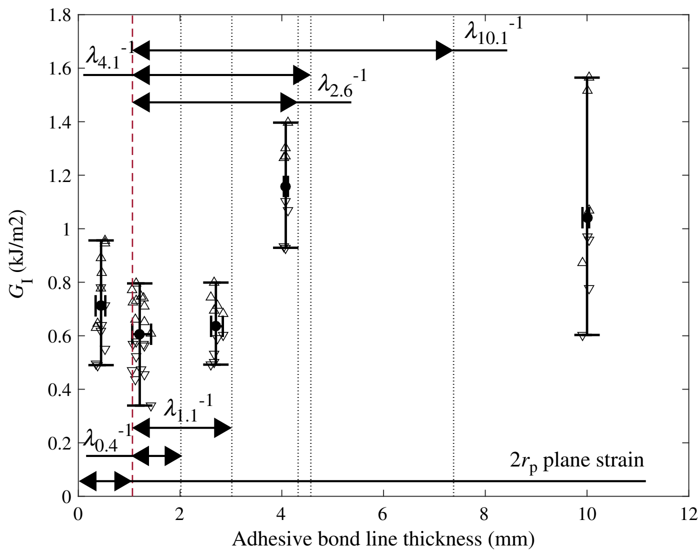

Fig. 18.8 Mode I fracture energy as a function of adhesive thickness. Two error bars are also plotted, giving the range of scatter on the thickness and G_I. The *red dashed line* gives the limit of $2r_p$ considering plane strain conditions. The *black dashed lines* give the limit of $2r_p + \lambda_{j-\exp}^{-1}$, where $j = 0.4, 1.1, 2.6, 4.1, 10.1$ mm, and the $\lambda_{j-\exp}^{-1}$ is the length of the elastic tensile stress region ahead of the crack tip estimated experimentally [50].

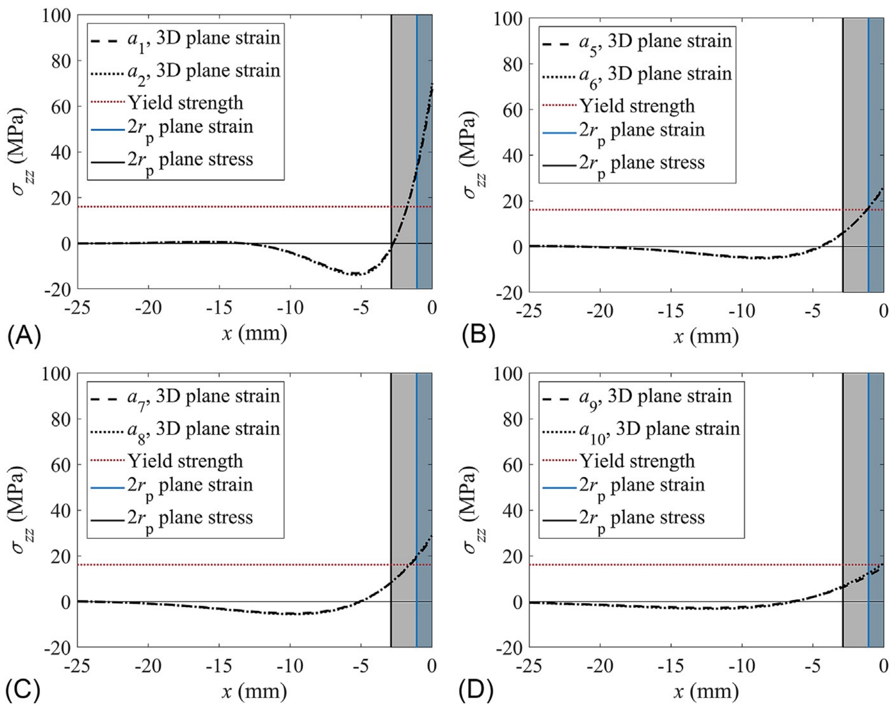

Fig. 18.9 Peel stresses ahead of the crack tip (located at $x = 0$). Two arbitrary points in the propagation region were selected for each representative specimen: crack length and load a_i, P_i respectively [50]. (A) $t_a = 2t = 0.4$ mm: σ_{zz}; (B) $t_a = 2t = 2.6$ mm: σ_{zz}; (C) $t_a = 2t = 4.1$ mm: σ_{zz}; (D) $t_a = 2t = 10.1$ mm: σ_{zz}.

18.4.1.4 Explaining fracture energy trend

Fig. 18.10 shows a schematic illustration of Mode I fracture energy as a function of adhesive thickness as stated by Kinloch and Shaw [5]. If applied to the case study hereby presented, the highest Mode I fracture toughness would be expected in the specimens with 1.1 mm adhesive thickness because $2t \approx 2r_\mathrm{p}$ ($2r_\mathrm{p} = 1.08$ mm), and decrease from 1.1 to 0.4 mm and from 1.1 to 10.1 mm. Although this is not the case for the bondline investigated in this case study, because 4.1 mm adhesive thickness results in the highest toughness as shown in Fig. 18.8, the theory can still support the overall trend while the stress fields ahead of the crack tip previously presented give interesting insights in to the deformation zone ahead of the crack tip.

In the specimens with thin bondlines of 0.4 mm, the effect of the adherend constraint is more pronounced, leading to higher confinement of the crack tip and higher local peel stresses. This is clearly shown in Fig. 18.9A with the highest peel stresses ahead of the crack tip in comparison with the remaining adhesive thicknesses and the expansion of the plastic deformation zone length higher than $2r_\mathrm{p}$ (plane strain conditions), resulting in a more elongated deformation zone with an elliptical shape, as reported by Kinloch and Shaw [5].

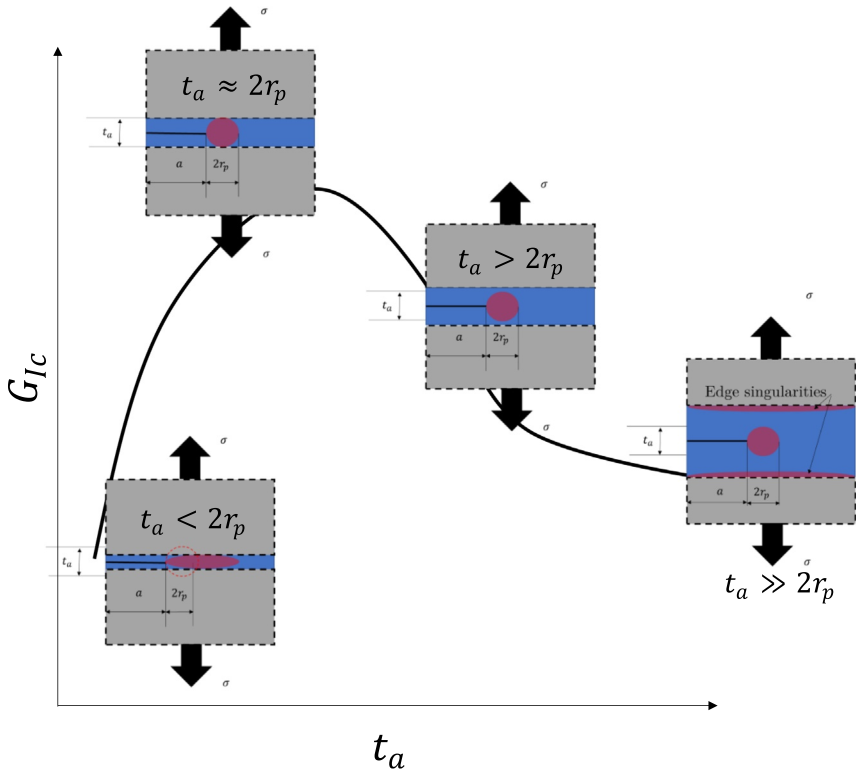

Fig. 18.10 Schematic illustration of Mode I fracture toughness as a function of adhesive thickness.
Adopted from A.J. Kinloch, S.J. Shaw, The fracture resistance of a toughened epoxy adhesive, J. Adhes. 12 (1) (1981) 59–77.

By increasing the bondline thickness to 2.6 mm, the adherend constraint gets smaller. This is seen in Fig. 18.9B in which the plastic deformation zone length decreases in comparison with 0.4 mm and it seems to converge to $2r_p$ (plane strain). In the range of bondline thicknesses of 0.4 to 2.6 mm, an increase on the average value of G_{Ic} as the physical constraint becomes less pronounced for thicker bondlines and, naturally, the deformation zone becomes larger in volume. However, the experimental results show a different trend. Similar average G_I values are obtained in the range of a 0.4–2.6 mm thick adhesive layer. It is important to note that the failure surfaces and crack paths present some differences. In the thinnest specimens, the surfaces displayed several densely packed peaks (Fig. 18.7A) characteristic for high stress triaxiality. For the thicker specimens of bondlines of 1.1 and 2.6 mm, the failure surfaces appear smoother and the changes on the crack path plane location might have prevented the full development of the deformation zone, leading in the end to similar results of G_I. Despite the fact that λ_{exp}^{-1} increases with the bondline thickness as shown is Fig. 18.8, this seems not to affect the average value of G_I in the bondline thicknesses range of 0.4–2.6 mm, which shows that energy dissipation mainly occurred in the plastic deformation zone.

In the specimens with a bondline of 4.1 mm, the adherend constraining effect should get even lower and the deformation zone should be fully developed, leading to higher energy dissipation before crack propagation, and consequently, higher G_I values. There was indeed an increase of approximately 84% in the average value of G_I from a bondline of 2.6 mm to a bondline of 4.1 mm, resulting in the joint with highest toughness. According to Kinloch and Shaw [5], the plastic deformation zone for this bondline thickness should have a height equal to $2r_p$ and a length longer than $2r_p$. The results in Fig. 18.9C agree with this theory regarding the increase in the length of the deformation zone. However, it should be noted that these predictions of the peel stresses assume perfectly cohesive crack propagation (i.e., at the midthickness of the bondline), which is not representative of the real crack path profile of the 4.1 mm thick adhesive bond line specimens (see Fig. 18.7D). In fact, the change on the crack plane must have affected the shape, size, and direction of the deformation zone, namely in the regions where the crack propagated close to one of the interfaces. Consequently, the real deformation zone length might be different from the estimated. Nevertheless, it seems that the deformation zone could develop more in the specimens with a bondline thickness of 4.1 mm than in the ones with a 2.6 mm thick adhesive bondline, as shown by the higher average G_I value obtained.

Finally, in the specimens with a bondline of 10.1 mm, the crack grew alternating between the two interfaces (but always within the adhesive layer as observed by the naked eye and confirmed by attenuated total reflectance Fourier transform infrared (ATR-FTIR) spectroscopy surface analysis [53]). Such bondlines, following Eq. (18.21) and Fig. 18.9, experience the lowest peel stresses; however, as shown in Fig. 18.4, they are the most likely to localize shear stresses near corners and edges. Consequently, the crack onset and the propagation are occurring most likely under mixed-mode conditions, breaking the symmetry conditions of the DCB configuration. As a consequence of the crack path location, the deformation zone was physically constrained just in one side, which might have reduced its size, and, subsequently, the Mode I fracture toughness. The estimation of λ_{exp}^{-1} and the plastic deformation zone from Fig. 18.9D might not be representative of the experiment due to the crack plane location.

The research done in the past has proved that there is a dependence of the fracture energy of adhesive joints on bonding thickness, regardless of the nature of the adhesives. In the present case study, the average Mode I fracture toughness, $G_{I\ av.}$, presented similar values for the specimens with adhesive bondline thicknesses in the range of 0.4–2.6 mm, and it increased by approximately 63% for the joints of a 4.1 mm thick bondline. A further increase in the thickness of the adhesive layer led to a decrease of about 10% in $G_{I\ av.}$ (in comparison with the 4.1 mm thick bond layer). These results show that the increase in bond thickness does not always lead to an increase in the critical fracture energy. This is consistent with the outlined theoretical framework. The trend of these results can be attributed to: (a) the crack path, which influences the stress field ahead of the crack tip and, consequently, the size of the deformation zone, and (b) the differences in the fracture surfaces' topography.

18.4.1.5 Strain rate dependency

While testing adhesive joints of different thicknesses, a common approach is to use a similar rate of applied displacement. Bearing in mind that the adhesives are polymers usually prone to time-dependent phenomena, maintaining the rate of loading while testing different adhesive thicknesses can result in misinterpretation. It is important to note the relationship between the strain rate and the adhesive thickness. Recalling the case depicted in Fig. 18.3B, undeformable adherends bonded with a relatively soft adhesive of thickness t_a. The strain in the thickness direction z experienced by the adhesive is given by:

$$\epsilon_{zz} = \frac{w(x)}{t_a} = \frac{w_t - w_b}{t_a}. \tag{18.24}$$

(Recall that w_t and w_b are displacements of the top and bottom adherends—see Fig. 18.2) Differentiating this formula with respect to time, the strain rate is given by:

$$\dot{\epsilon}_{zz} = \frac{\dot{w}(x)}{t_a} \tag{18.25}$$

This shows that as the adhesive thickness t_a increases, the strain rate decreases in the exact same proportions, which bears severe consequences [54]. The simple linear relation is, however, not always the case. For instance, for DCB testing, the rate of crack growth and strain rate at the crack tip are a function of crack position and changes during testing, that is, the rates are slower at the end of the test than in the beginning [55]. Significant research has been done on strain rate dependence of the Mode I fracture energy. However, the literature is not unanimous on their relation. Blackman et al. [56, 57] have reported a decrease in fracture toughness under Mode I loading G_{Ic} with increased strain rate, but the majority of researchers report the opposite, an increase of fracture toughness with the increase in strain rate [58–61]. A phenomenological model, [62] based on the fracture process zone size dependence on time, indicates that for shorter times, and thus, higher strain rates, the process zone converges toward elastic solution. For longer times and lower rates, the process zone can easily grow without an actual growth of the crack. Thus, if one uses the apparent crack length approach (crack position observed from the side with a camera), the extension of the process zone will lead to higher deformations and recorded displacements while keeping the crack length constant at a given force, thus overestimating the fracture energy. On the contrary, by using the effective crack length approach, the extension of the process zone will be interpreted as an extension of a_e that is counteracting the increased displacements. For the DCB case study here presented, the strain rate decreases as the adhesive thickness increases. Taking into account the results from the majority of the literatures, this could imply that the decrease in the fracture toughness from 1.1 to 2.6 mm and from 4.1 to 10.1 mm could be partly due to the difference in the strain rates. Nevertheless, all the cited literature varied the strain rate by varying the displacement crosshead rate of the tests while the adhesive thickness was kept constant. In the case study here presented, the strain rate varied by varying the adhesive thickness while the displacement crosshead rate of the test was kept constant. Further studies are needed to prove whether the similitude between these two holds.

18.4.2 Crack initiation competition in thick bonded joints

With a bondline thickness on the centimeter scale, one feature to be recognized is the stress gradient that arises at the bi-material adhesive-adherend edges and corners [15, 16, 38, 63]. The differences in material properties and geometry singularities at these locations result in opening stresses, as shown in Eq. (18.9), that can trigger fracture onset. Interestingly, this feature can be used as a fracture trigger to increase the fracture toughness of the bonded joint. The control over the number and the location of the

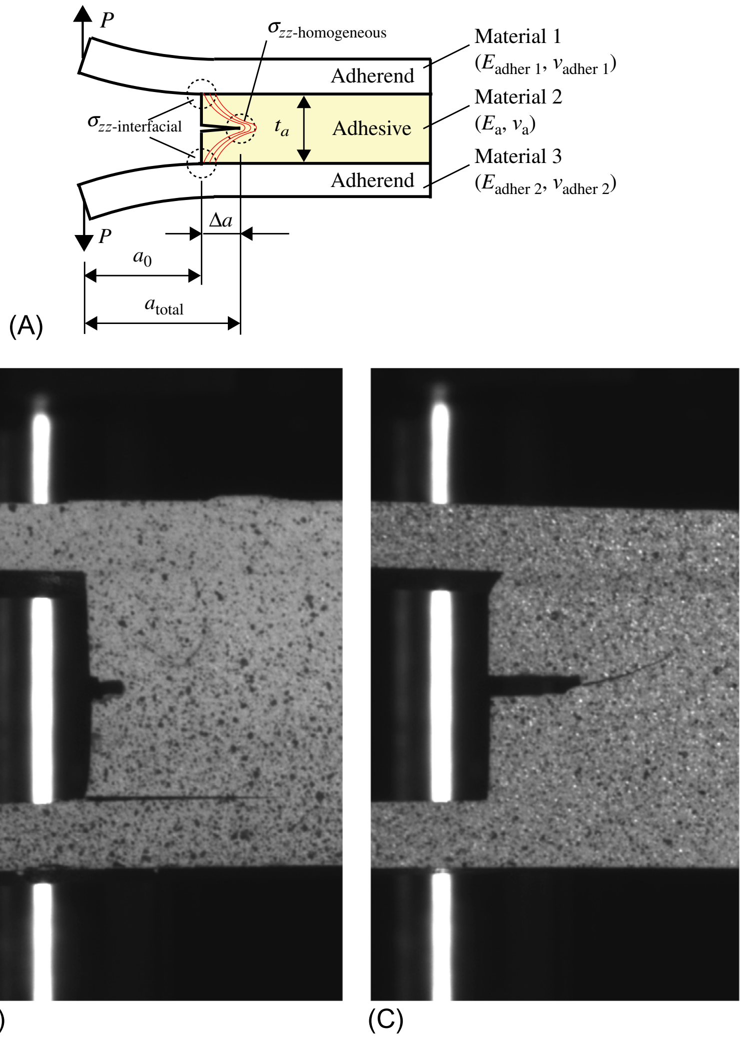

Fig. 18.11 (A) Fracture scenario in study: influence of Δa length on fracture onset in adhesive joint with finite thickness adherends under global Mode I loading; (B) Fracture onset close to the interface; (C) Fracture onset at the precrack [40].

plastic zones resulting from fracture onset in elasto-plastic adhesives can be of high benefit to increase and tailor the resistance to fracture and overall performance of the joint.

In this section, the relation between fracture initiation at the corner and bi-material singularities and the fracture initiation at the midthickness adhesive is studied. Fig. 18.11A represents the fracture scenario at hand. The case study here investigated considers an adhesive of thickness $t_a = 2t \approx 10$ mm. A precrack of length Δa is cut at midthickness of the adhesive bondline. Steel and glass fibre reinforced polymer (GFRP) were used as adherends. DCB bonded joints made of single adherend material (steel-steel and GFRP-GFRP) and bi-material (steel-GFRP) adherends bonded with a structural epoxy adhesive were tested. Details of the manufacturing and experimental setup can be found in [40].

Fig. 18.11B and C shows examples of the two possible fracture onsets encountered. The fracture competition between the corner singularities and the precrack can be described as the fracture onset will occur at the precrack tip if Δa is sufficiently large to create a singular stress field around the precrack tip, in which the threshold stress is reached prior than at the bi-material edges and corners. In the subsequent sections the roles of the adherend-adhesive modulus mismatch and the precrack length in this crack onset competition are demonstrated.

18.4.2.1 Role of adherend-adhesive modulus mismatch

At the adherend-adhesive edge, stresses arise due to material mismatch the values of which are dependent upon the material and geometrical properties. This dependency can be quantified using the Dundurs [15] parameters α and β, previously presented by Eqs. (18.10) and (18.11), respectively (1 = adherend and 2 = adhesive). The parameter α can be interpreted as a measure of the stiffness dissimilarity between the two materials: for $\alpha > 0$, the adherend material is rigid relative to the adhesive. The parameter β is related to the oscillatory crack path near the crack onset. Table 18.1 lists both parameters for the case study at hand for the steel-epoxy as well as for the GFRP-epoxy interface.

Both Dundurs parameters are higher for the steel-epoxy interface, which means that, in the case of fracture onset close to the interface at bi-material bonded joints, the fracture location is more likely to occur at the steel-epoxy interface, the one with the highest adherend-adhesive modulus mismatch. Experimental and numerical evidence of this fact is confirmed in [53] and [40], respectively. Fig. 18.12 shows the

Table 18.1 Dundurs parameters for different material combinations under plane strain conditions [40].

Adherend/ adhesive	G_{adher} (GPa)	G_a (GPa)	ν_{adher} (–)	ν_a (–)	α (–)	β (–)
Steel/epoxy	80769	752	0.300	0.33	0.98	0.25
GFRP/epoxy	3897	752	0.252	0.33	0.65	0.15

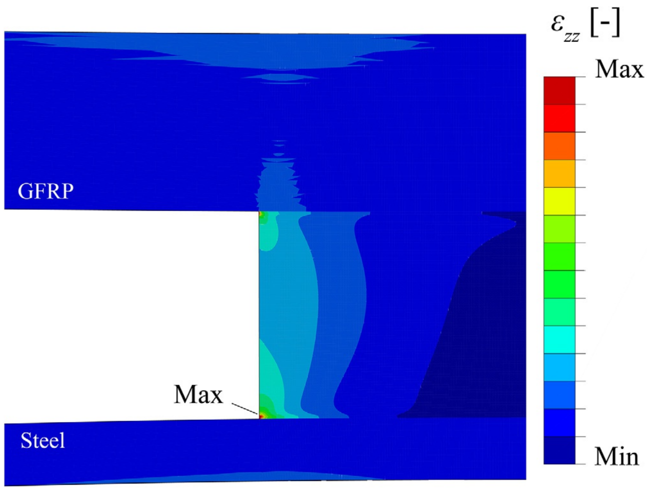

Fig. 18.12 Evolution of strain field, ε_{zz} for bi-material bonded joint GFRP-steel. No precrack is modeled, $\Delta a = 0$ mm.
Adapted from R.L. Fernandes, M.K. Budzik, R. Benedictus, S. Teixeira de Freitas, Multimaterial adhesive joints with thick bond-lines: crack onset and crack deflection, Compos. Struct. 266 (2021) 113687.

numerical evidence. The strain distribution is not symmetric and the highest strain values are found close to the steel-epoxy interface.

18.4.2.2 Role of precrack length

In this section, the role of $\Delta a \neq 0$ mm in the fracture onset locus of thick bi-material bonded joints is analyzed.

Up to a certain bondline thickness, the fracture onset is dominated by a singular stress field around the existing precrack tip in the adhesive. However, for thicker bondlines, geometric and material discontinuities, such as corners and adherend-adhesive interfaces create local stresses where the failure might occur first; see Figs. 18.5 and 18.11B. To avoid this fracture onset locus to fully explore the cohesive properties of the adhesive, a certain critical precrack length Δa_{crit} must be fulfilled such that the threshold stress is attained first at the precrack tip rather than at corners. The criterion to define Δa_{crit} follows the Griffith's diffusion line approach, which proposes that for a crack in a homogeneous material of well-defined length a, a region of material adjacent to the free surfaces is unloaded [64]. Applying this concept to adhesive joints translates into Δa being sufficiently long such that the corners near the interfaces are unloaded, as shown in Fig. 18.11A by the red diffusion lines.

According to [65], in an infinite plate with a crack, the unloaded region is approximated by a triangle with the base length corresponding to Δa and a height of $2\pi\Delta a$. For the case study here presented in Fig. 18.11A, this would mean that as long as $t_a = 2t \geqslant 4\pi\Delta a$, the corners are unloaded and the crack onsets at the crack tip. It is made clear that the Δa_{crit} is dependent on the bondline thickness. To demonstrate this relation, experimental tests and numerical simulations were performed varying Δa. Fig. 18.13 shows the resulting strain field obtained numerically (refer to [40] for details on the numerical simulations).

From the experimental results, it was found that for $r_p < t$ and $\Delta a > 0$, a ratio of $\frac{\lambda^{-1}}{\Delta a} \leqslant 2$ leads to cohesive fracture onset (i.e., at mid-adhesive thickness). Replacing λ by Eq. (18.19) with $t_a = 2t$, the empirical relation for cohesive fracture onset can also be expressed as $(8E_aB/E_x^fI)(\Delta a_{crit.})^4 \geqslant 2t$, so that for a given material mismatch, for the DCB geometry, $(\Delta a_{crit.}/h_{adher})^4 \sim (t/h_{adher})$ is the scaling relation for transition into cohesive fracture onset.

In summary, for $\Delta a < \Delta a_{crit.}$, the stress singularity near the bi-material corner rules over the stress singularity at the precrack tip. The bi-material corner with the highest modulus mismatch, characterized by the highest Dundurs parameters, dictates the region of fracture initiation; for $\Delta a \geqslant \Delta a_{crit.}$ the stress singularity at the precrack tip is dominant, resulting in cohesive fracture onset.

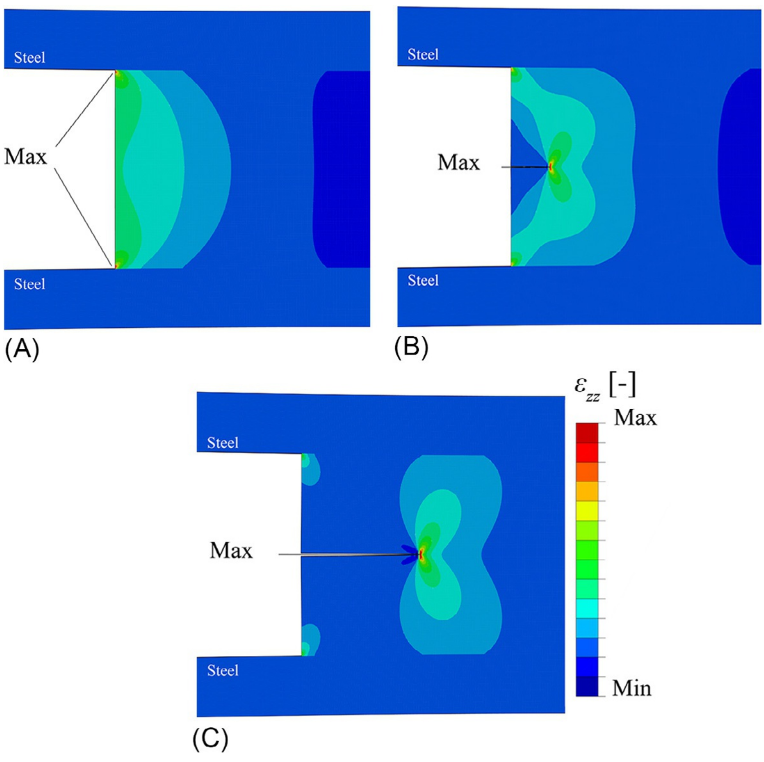

Fig. 18.13 Evolution of strain field, ε_{zz}, in steel-steel joint with increasing Δa. (A) $\Delta a = 0$ mm; (B) $\Delta a = 2$ mm; (C) $\Delta a = 6$ mm.
Adapted from R.L. Fernandes, M.K. Budzik, R. Benedictus, S. Teixeira de Freitas, Multimaterial adhesive joints with thick bond-lines: crack onset and crack deflection, Compos. Struct. 266 (2021) 113687.

18.5 Summary and future directions

Conventionally, the bondline thickness has been regarded as a consequence or medium to address some of the performance requirements (thin, stiff bondlines for aerospace) or to address manufacturing process limitations, mainly tolerances (thicker bondlines used in transportation and civil engineering applications). With the development of wind energy as well as marine and civil engineering markets and the focus on lightweight structures, thick bondlines became also a necessity. The new, thicker bondlines became a new and critical length scale for a joint and require different analysis and evaluation due to different load transfer mechanisms and failure modes. These have not always been adopted and are not part of either standard or certification procedure. However, the increased thickness does not need to be considered as a consequence but rather a design feature to be explored. This additional new dimension opens new design routes and expands the design freedom. The adhesive thickness can be used to optimize properties, shape load response, and add functionalities; it can also lead to the development of greener solutions with new materials and limited usage. Recently, use of the mechanical metamaterials as a substitution for traditional bondlines has been proposed [66]. While offering significant volumes, such systems can weigh only a percentage of today's thick bondline systems while maintaining satisfactory mechanical properties. Only time will tell if such a geometrical approach gains widespread acceptance.

References

[1] G.P. Anderson, S.J. Bennett, K.L. DeVries, Analysis and testing of adhesive bonds, NASA, 1977. Tech. rep.

[2] M.K. Budzik, M. Wolfahrt, P. Reis, M. Kozłowski, J. Sena-Cruz, L. Papadakis, M. Nasr Saleh, K.V. Machalicka, S. Teixeira de Freitas, A.P. Vassilopoulos, Testing mechanical performance of adhesively bonded composite joints in engineering applications: an overview, J. Adhes. 98 (14) (2021) 2133–2209.

[3] S. Mostovoy, E.J. Ripling, Fracture toughness of an epoxy system, J. Appl. Polym. Sci. 10 (9) (1966) 1351–1371.

[4] S. Mostovoy, E.J. Ripling, Effect of joint geometry on the toughness of epoxy adhesives, J. Appl. Polym. Sci. 15 (3) (1971) 661–673.

[5] A.J. Kinloch, S.J. Shaw, The fracture resistance of a toughened epoxy adhesive, J. Adhes. 12 (1) (1981) 59–77.

[6] S. Mall, G. Ramamurthy, Effect of bond thickness on fracture and fatigue strength of adhesively bonded composite joints, Int. J. Adhes. Adhes. 9 (1) (1989) 33–37.

[7] C. Yan, Y.-W. Mai, L. Ye, Effect of bond thickness on fracture behaviour in adhesive joints, J. Adhes. 75 (1) (2001) 27–44.

[8] L.F. Kawashita, A.J. Kinloch, D.R. Moore, J.G. Williams, The influence of bond line thickness and peel arm thickness on adhesive fracture toughness of rubber toughened epoxy-aluminium alloy laminates, Int. J. Adhes. Adhes. 28 (4–5) (2008) 199–210.

[9] P. Davies, L. Sohier, J.-Y. Cognard, A. Bourmaud, D. Choqueuse, E. Rinnert, R. Créac'hcadec, Influence of adhesive bond line thickness on joint strength, Int. J. Adhes. Adhes. 29 (7) (2009) 724–736.

[10] J.M. Arenas, J.J. Narbón, C. Alía, Optimum adhesive thickness in structural adhesives joints using statistical techniques based on Weibull distribution, Int. J. Adhes. Adhes. 30 (3) (2010) 160–165.
[11] G. Ji, Z. Ouyang, G. Li, On the interfacial constitutive laws of mixed mode fracture with various adhesive thicknesses, Mech. Mater. 47 (2012) 24–32.
[12] M.K. Budzik, J. Jumel, M.E.R. Shanahan, 4-Point beam tensile test on a soft adhesive, Mater. Des. 46 (2013) 134–141.
[13] D.J. Alner, Aspects of Adhesion, vol. 6, University of London Press, 1965.
[14] J. Dundurs, T. Mura, Interaction between an edge dislocation and a circular inclusion, J. Mech. Phys. Solids 12 (3) (1964) 177–189.
[15] D.B. Bogy, On the problem of edge-bonded elastic quarter-planes loaded at the boundary, Int. J. Solids Struct. 6 (9) (1970) 1287–1313.
[16] E.D. Reedy, T.R. Guess, Interface corner failure analysis of joint strength: effect of adherend stiffness, Int. J. Fract. 88 (4) (1997) 305–314.
[17] S. Krenk, Energy release rate of symmetric adhesive joints, Eng. Fract. Mech. 43 (4) (1992) 549–559.
[18] W.D. Bascom, R.L. Cottington, R.L. Jones, P. Peyser, The fracture of epoxy-and elastomer-modified epoxy polymers in bulk and as adhesives, J. Appl. Polym. Sci. 19 (9) (1975) 2545–2562.
[19] B. Zhao, Z.-H. Lu, Y.-N. Lu, Closed-form solutions for elastic stress-strain analysis in unbalanced adhesive single-lap joints considering adherend deformations and bond thickness, Int. J. Adhes. Adhes. 31 (6) (2011) 434–445.
[20] L.F.M. Da Silva, T.N.S.S. Rodrigues, M.A.V. Figueiredo, M.F.S.F. De Moura, J.A.G. Chousal, Effect of adhesive type and thickness on the lap shear strength, J. Adhes. 82 (11) (2006) 1091–1115.
[21] M. Goland, E. Reissner, The stresses in cemented joints, J. Appl. Mech. 11 (1) (1944) A17–A27.
[22] D.A. Dillard, Fundamentals of Stress Transfer in Bonded, Elsevier, 2002.
[23] W. Flügge, Tensor Analysis and Continuum Mechanics, vol. 4, Springer, 1972.
[24] T. Pardoen, T. Ferracin, C.M. Landis, F. Delannay, Constraint effects in adhesive joint fracture, J. Mech. Phys. Solids 53 (9) (2005) 1951–1983.
[25] F. Van Loock, M.D. Thouless, N.A. Fleck, Tensile fracture of an adhesive joint: the role of crack length and of material mismatch, J. Mech. Phys. Solids 130 (2019) 330–348.
[26] A.A. Griffith, M. Eng, The phenomena of rupture and flow in solids, Phil. Trans. R. Soc. Lond. A 221 (582–593) (1921) 163–198.
[27] P.P. Gillis, J.J. Gilman, Double-cantilever cleavage mode of crack propagation, J. Appl. Phys. 35 (3) (1964) 647–658.
[28] E.J. Ripling, S. Mostovoy, R.L. Patrick, Measuring fracture toughness of adhesive joints, Mater. Res. Stand 4 (3) (1964) 129–134.
[29] K. Kondo, Analysis of double cantilever beam specimen, Adv. Compos. Mater. 4 (4) (1995) 355–366.
[30] A.N. Gent, Fracture mechanics of adhesive bonds, Rubber Chem. Technol. 47 (1) (1974) 202–212.
[31] H.M. Westergaard, Bearing pressures and cracks, J. Appl. Mech. 6 (2) (1939) A49–A53.
[32] H.M. Westergaard, Theory of Elasticity and Plasticity, vol. 367, Harvard University Press Cambridge, 1952.
[33] G.C. Sih, On the Westergaard method of crack analysis, Int. J. Fract. Mechanics 2 (4) (1966) 628–631.

[34] G.R. Irwin, Analysis of stresses and strains near the end of a crack traversing a plate, J. Appl. Mech. 24 (1957) 361–364.

[35] E.H. Andrews, A.J. Kinloch, Mechanics of adhesive failure. II, Proc. R. Soc. Lond. A. Math. Phys. Sci. 332 (1590) (1973) 401–414.

[36] P. Martiny, F. Lani, A.J. Kinloch, T. Pardoen, A multiscale parametric study of mode I fracture in metal-to-metal low-toughness adhesive joints, Int. J. Fract. 173 (2) (2012) 105–133.

[37] S.R. Ranade, Y. Guan, D.C. Ohanehi, J.G. Dillard, R.C. Batra, D.A. Dillard, A tapered bondline thickness double cantilever beam (DCB) specimen geometry for combinatorial fracture studies of adhesive bonds, Int. J. Adhes. Adhes. 55 (2014) 155–160.

[38] A.R. Akisanya, C.S. Meng, Initiation of fracture at the interface corner of bi-material joints, J. Mech. Phys. Solids 51 (1) (2003) 27–46.

[39] A. Dimitrov, H. Andrä, E. Schnack, Efficient computation of order and mode of corner singularities in 3D-elasticity, Int. J. Numer. Methods Eng. 52 (8) (2001) 805–827.

[40] R.L. Fernandes, M.K. Budzik, R. Benedictus, S. Teixeira de Freitas, Multi-material adhesive joints with thick bond-lines: crack onset and crack deflection, Compos. Struct. 266 (2021) 113687.

[41] J.J. Benbow, F.C. Roesler, Experiments on controlled fractures, Proc. Phys. Soc. Sect. B 70 (2) (1957) 201.

[42] B.R.K. Blackman, H. Hadavinia, A.J. Kinloch, M. Paraschi, J.G. Williams, The calculation of adhesive fracture energies in mode I: revisiting the tapered double cantilever beam (TDCB) test, Eng. Fract. Mech. 70 (2) (2003) 233–248.

[43] M. Budzik, J. Jumel, M.E.R. Shanahan, Adhesive compliance effect in mode I separation: profilometry approach, Int. J. Adhes. Adhes. 31 (3) (2011) 135–145.

[44] S.P. Timoshenko, S. Woinowsky-Krieger, Theory of Plates and Shells, McGraw-Hill, 1959.

[45] M.A. Biot, Bending of an infinite beam on an elastic foundation, J. Appl. Math. Mech. 2 (3) (1922) 165–184.

[46] G.J. Spies, The peeling test on redux-bonded joints: a theoretical analysis of the test devised by aero research limited, Aircr. Eng. Aerosp. Technol. 25 (3) (1953) 64–70.

[47] A.D. Kerr, Elastic and viscoelastic foundation models, J. Appl. Mech. 31 (3) (1964) 491–498.

[48] D.A. Dillard, B. Mukherjee, P. Karnal, R.C. Batra, J. Frechette, A review of Winkler's foundation and its profound influence on adhesion and soft matter applications, Soft Matter 14 (19) (2018) 3669–3683.

[49] M.F. Kanninen, An augmented double cantilever beam model for studying crack propagation and arrest, Int. J. Fract. 9 (1) (1973) 83–92.

[50] R. Lopes Fernandes, S. Teixeira de Freitas, M.K. Budzik, J.A. Poulis, R. Benedictus, From thin to extra-thick adhesive layer thicknesses: fracture of bonded joints under mode I loading conditions, Eng. Fract. Mech. 218 (2019), 106607.

[51] B. Chen, D.A. Dillard, J.G. Dillard, R.L. Clark Jr, Crack path selection in adhesively-bonded joints: the role of material properties, J. Adhes. 75 (4) (2001) 405–434.

[52] B. Chen, D.A. Dillard, The effect of the T-stress on crack path selection in adhesively bonded joints, Int. J. Adhes. Adhes. 21 (5) (2001) 357–368.

[53] R. Lopes Fernandes, S. Teixeira de Freitas, M.K. Budzik, J.A. Poulis, R. Benedictus, Role of adherend material on the fracture of bi-material composite bonded joints, Compos. Struct. 252 (2020), 112643.

[54] C.M. Landis, T. Pardoen, J.W. Hutchinson, Crack velocity dependent toughness in rate dependent materials, Mech. Mater. 32 (11) (2000) 663–678.

[55] S. Heide-Jørgensen, M.K. Budzik, Effects of bondline discontinuity during growth of interface cracks including stability and kinetic considerations, J. Mech. Phys. Solids 117 (2018) 1–21.

[56] B.R.K. Blackman, A.J. Kinloch, F.S. Rodriguez Sanchez, W.S. Teo, J.G. Williams, The fracture behaviour of structural adhesives under high rates of testing, Eng. Fract. Mech. 00137944, 76 (18) (2009) 2868–2889, https://doi.org/10.1016/j.engfracmech.2009.07.013.

[57] A. Karac, B.R.K. Blackman, V. Cooper, A.J. Kinloch, S. Rodriguez Sanchez, W.S. Teo, A. Ivankovic, Modelling the fracture behaviour of adhesively-bonded joints as a function of test rate, Eng. Fract. Mech. 00137944, 78 (6) (2011) 973–989, https://doi.org/10.1016/j.engfracmech.2010.11.014.

[58] I. Georgiou, A. Ivankovic, A.J. Kinloch, V. Tropsa, Rate dependent fracture behaviour of adhesively bonded joints, in: European Structural Integrity Society, vol. 32, Elsevier, 2003, pp. 317–328, https://doi.org/10.1016/S1566-1369(03)80105-X.

[59] T. Carlberger, A. Biel, U. Stigh, Influence of temperature and strain rate on cohesive properties of a structural epoxy adhesive, Int. J. Fract. 03769429, 155 (2) (2009) 155–166,- https://doi.org/10.1007/s10704-009-9337-4.

[60] M. May, O. Hesebeck, S. Marzi, W. Böhme, J. Lienhard, S. Kilchert, M. Brede, S. Hiermaier, Rate dependent behavior of crash-optimized adhesives–experimental characterization, model development, and simulation, Eng. Fract. Mech. 00137944, 133 (2015) 112–137, https://doi.org/10.1016/j.engfracmech.2014.11.006.

[61] C.S.P. Borges, P.D.P. Nunes, A. Akhavan-Safar, E.A.S. Marques, R.J.C. Carbas, L. Alfonso, L.F.M. Silva, A strain rate dependent cohesive zone element for mode I modeling of the fracture behavior of adhesives, Proc. Inst. Mech. Eng. L J. Mater. Des. Appl. 20413076, 234 (4) (2020) 610–621, https://doi.org/10.1177/1464420720904026.

[62] J. Jumel, S. Chauffaille, M.K. Budzik, M.E. Shanahan, J. Guitard, Viscoelastic foundation analysis of single cantilevered beam (SCB) test under stationary loading, Eur. J. Mech. A Solids 39 (2013) 170–179.

[63] J.W. Hutchinson, M.E. Mear, J.R. Rice, Crack paralleling an interface between dissimilar materials, J. Appl. Mech. 54 (1987) 828–832.

[64] N. Perez, Fracture Mechanics, Springer, 2017, https://doi.org/10.1007/b118073.

[65] Z.P. Bazant, L. Cedolin, Stability of Structures: Elastic, Inelastic, Fracture and Damage Theories, World Scientific, 2010.

[66] A.E. Athanasiadis, M.A. Dias, M.K. Budzik, Can confined mechanical metamaterials replace adhesives? Extreme Mech. Lett. 48 (2021) 101411.